Radial Flow Force at the Annular Orifice of a Two-Dimensional Hydraulic Servo Valve

QIANQIAN LU[1,2], **JONNA TIAINEN**[2], **MEHRAN KIANI-OSHTORJANI**[2], **AND JIAN RUAN**[3]

[1]School of Engineering, Zhejiang University City College, Hangzhou 310015, China
[2]School of Energy Systems, Lappeenranta–Lahti University of Technology (LUT), 53850 Lappeenranta, Finland
[3]College of Mechanical Engineering, Zhejiang University of Technology, Hangzhou 310023, China

Corresponding author: Qianqian Lu (luqianqian@zucc.edu.cn)

ABSTRACT A two-dimensional hydraulic servo valve is an innovative servo control element that provides hydraulic systems with a high power-to-weight ratio, great anti-pollution potential, and superior static and dynamic characteristics. The spool of such a valve is subject to two degrees of freedom: rotation around and sliding along the spool axis, to accomplish both pilot control and flow amplifier functions. The structure of the spool at the main stage is similar to that of a traditional slide valve wherein the asymmetrical distribution of the oil paths manufactured in the valve body produces circumferential unevenness in the radial flow force to the spool at the annular orifice, in line with the momentum theory. Three-dimensional computational fluid dynamics analysis of the flow field revealed that the radial flow force at the annular orifice increases sharply with inlet flow velocity and decreases as the orifice opening grows, while changes in outlet pressure do not affect the levels or distribution of this force. Also, net radial force at the annular orifice increases with both inlet velocity and opening size. The paper presents results demonstrating that the net radial force from fluid flow through the orifice could increase friction resistance and cannot be safely ignored, especially under high-flow-rate conditions.

INDEX TERMS CFD, net radial force, pressure distribution, radial flow force, slide valve.

I. INTRODUCTION

A two-dimensional (2D) hydraulic servo valve is a control unit whose fast dynamic response and capacity for precise flow control play a critical role in determining the overall performance of the hydraulic servo system. This type of servo valve represents a novel solution for pilot control of a two-stage valve, combining the pressure control handled by the pilot stage and the flow amplification through the main stage into a single-spool operation. Its inventor, Ruan [1], proved that a 2D servo valve overcomes the drawbacks related to a nozzle flapper servo valve's sensitivity to oil contamination and a jet pipe servo valve's high pilot leakage. He established the stability criteria and analysed the structural parameters that affect the static and dynamic characteristics of a 2D servo flow valve [2]. Meanwhile, the nonlinearities, such as electromagnetic saturation and hysteresis, are greatly reduced

The associate editor coordinating the review of this manuscript and approving it for publication was Tao Wang.

by application of a stage control method to the electrical-to-mechanical actuator [3]. Li *et al.* [4] implemented a tracking control algorithm for the electro-mechanical converter, which helps enhance the dynamic characteristics of the 2D servo valve: the −3 dB frequency of the valve was 210 Hz, and the rise time for step response was approximately 8 ms.

A 2D servo valve with both rotary and linear motions on a single spool offers the benefits of a high power-to-weight ratio, high anti-pollution capacity, and response sensitivity. Alongside this type of valve, such components as 2D high-speed on–off valves [5] and 2D proportional hydraulic valves [6], [7] employ the same operation mechanism, designed to expand the branching of 2D hydraulic valves and enrich hydraulic control units' products. For further improving the power-to-weight ratio and improving the efficiency of 2D servo valves, it is essential to study the flow forces and frictional resistance acting on the spool, which are balanced with the driving force generated by the electro-hydraulic actuator.

The steady flow force is the force acting on the spool because of fluid flow through the valve, which has an important role in the control of high-hydraulic-power systems [8], [9]. Yuan and Li [8] studied fluid force in efforts to increase the agility of the spool such that fast spool response can be achieved without as much power from the actuator. They found that steady flow force can be reduced via the viscosity and non-metering flux effect. In other work, Herakovič [9] implemented geometric modification of the sliding spool and the valve socket to compensate for the axial flow forces by designing a conical form for the sliding spool at the inlet control edge, which helped to decrease fluid velocity at the outlet cross-section. Then, studying the flow force acting on the spool of a directional-control valve, Rajda and Lisowski [10] verified that the flow has very little influence on the axial flow force for the inflow path while being highly significant for the outflow path. In more recent research, Frosina *et al.* [11], [12] focused on simulation and calculation of axial flow forces within directional-control valves by comparing the stream lines under various spool displacement conditions and inlet flow rates. Their results indicated that the force values contingent on spool displacement create strong force oscillations when the spool was moved from zero to 2.8 mm.

Amirante *et al.* [13] confirmed the necessity of full three-dimensional (3D) computational fluid dynamics (CFD) investigation of fluid flow through proportional-type hydraulic directional-control valves, which can accurately predict the flow forces acting on the spool in aims of minimising the required driving forces. They also redesigned the central conical and lateral surfaces of the new spool and succeeded in reducing the actuation force by more than 10% from that of the commercial spool commonly used in four-way three-position directly operated valves at maximal opening for the given flow rate examined in the experimental verification [14]. Han *et al.* [15] studied the axial flow forces on the spool with a double U-groove structure of a cartridge valve. They found that the highest axial flow forces decreased by 10% with their groove-geometry optimisation. Xie *et al.* [16], in turn, investigated the steady axial flow force compensation of a converged-flow cartridge proportional valve. They optimised the spool structure by adding a damping tail to regulate the flow force acting on the spool and to diminish the negative impact of flow force without affecting the pressure drop between the inlet and outlet. In recent work, Li *et al.* [17] designed a damping flange for the spool of the same cartridge valve to compensate for the axial flow force. The optimal parameters for the damping flange were obtained via CFD analysis, and experimental testing revealed a 93% decrease in flow force after the damping flange determined to be optimal was implemented. Related work was carried out by Qu *et al.* [18], who reduced the steady flow force through their design of a turbine bucket profile in the spool groove of the electro-hydraulic proportional relief valve. The flow force increment with their optimised spool was smaller than that experienced with the original spool when the flow

was increased under various pressures. For instance, the flow force fell by 26.7% when the working pressure was 4 MPa.

Lugowski [19] modified the formulae for the flow forces on the basis of measurements of the pressure distribution near the orifice of spool-type hydraulic valves with and without a compensation structure. Furthermore, the sticking problem experienced by these valves was studied in light of the flow force and its distribution [20], and the motion function of the spool was established as creating non-sticking threshold conditions. Flow force was found to be influenced more by the valve opening than by the temperature, especially for small openings [21].

As the literature review above indicates, previous studies were focused mainly on the axial-flow force component. Many means of reducing or compensating for the axial flow force have been investigated in pursuit of more efficient hydraulic valves and lower energy costs, while the radial flow force has often been neglected or assumed to be axially symmetrical [19]–[21]. The fluid cavity and paths are not, in fact, axially symmetrical within the valve, so the radial flow force at the orifice must be influenced, and these forces do not cancel each other out.

Zhang *et al.* [22] studied the radial forces acting on the spool of a 2D valve and found this force to affect the spool of the 2D servo valve in three distinct ways – with regard to the cone profile of the spool shoulder, the eccentricity between the spool and sleeve, and the asymmetry of the spiral channels of the pilot stage. Clamping force caused by eccentricity at the pilot stage of the 2D electro-hydraulic proportional directional-control valve was investigated in studies by Liu and colleagues [6], who proved that the radial force can be reduced by cutting a flat plane over each high-pressure and low-pressure hole on the spool shoulder at the pilot stage – but at the expense of increasing leakage. In more recent work, Lu *et al.* [23] studied the radial flow force induced when the liquid passes through the helical orifices of the pilot stage of a 2D servo valve. They found that this force was affected by the flow rate and the helical orifice opening; moreover, the force increased with the flow rate and acted in the direction opposite the driving force.

The spool of a 2D servo valve is a sliding-type element, and its main stage is in charge of the flow rate, as is the case in most sliding-spool valves. The flow rate is controlled by the annular orifice formed by the spool and housing, and the flow force rises in direct proportion to the flow rate [9], opposite the driving force as noted above. All the above-mentioned studies focused on the characteristics of the axial flow force and on compensation methods to reduce that force so as to improve the ratio of the power to the sliding-valve density further. Researchers have assumed the radial flow forces to cancel themselves out because of the symmetrical structure. Again, the inner flow cavity of the valve is not entirely symmetrical, especially with the plate-mounting type. This is because the four or five oil ports and passages created in the housing are asymmetrically distributed in accordance

with the ISO 103772:1992 standard, which was reviewed and confirmed in 2017 [24].

When the fluid flows into the asymmetric fluid cavity and enters the annular orifice, the fluid's pressure and velocity are not uniformly distributed over the orifice, so the radial component of the flow force is not zero. This was verified by Rajda and Lisowski [10], who found the force in the two directions perpendicular to the spool axis to be 40 N and 28 N, for the inlet flow path, and the values were 252 N and 83 N for the outlet flow path, when the flow rate was 450 l/min. Moreover, the momentum theory assumes jet angle θ to be 69° [25], so the radial flow force expected is 2.6 times the axial flow force [20]. Such studies indicate that the radial force is affected by jet flow through the orifice. Therefore, it is important to examine the radial component of flow force because it has negative effects on the spool, as the frictional force comprises a Coulomb friction component produced by radial forces. The Coulomb friction forces must be avoided, because they could cause the dead-band span of a valve, and consequently demand more force potential from the electro-mechanical actuator. Studying the effect of both axial and radial flow forces on the spool is an important aspect of endeavours to minimise an actuator's power demands.

What this paper contributes to scholarship and practice is numerical examination of the radial flow force and discussion of that force's influence on a 2D servo valve. The results of our study highlight the importance of the radial flow force in the design of both 2D servo valves and traditional sliding valves. If both the axial and radial flow forces were minimised, the actuator's power requirements could be reduced, which would result in a higher power-to-weight ratio.

In the discussion below, the radial flow force at the annular orifice of the main stage in a 2D servo valve is considered, thus: Firstly, the structure and principle of operation are introduced. Then, Section 3 provides an illustration of our numerical model, based on the partial 3D flow domain. The influences of the orifice opening, outlet pressure, and flow rate on the radial flow force are discussed in the fourth section, followed by analysis of the net radial force acting on the spool. The paper concludes with a summary and suggestions for future work.

II. THE TWO-DIMENSIONAL VALVE
A. THE STRUCTURE AND PRINCIPLE
The main-stage structure of the spool inside the 2D servo valve studied is similar to that of traditional slide spools, and the five oil passages machined in to the housing are arranged asymmetrically. Therefore, the flow cavity formed by the spool and housing should affect the radial component of flow force at the annular orifice when fluid flows through it. Fig. 1 shows the structure of a 2D servo valve with a nominal size of 22 mm. The pilot stage of the valve is presented at the left in the smaller rectangular box, and the main stage is outlined in the right-hand rectangular area. When the fluid flows into port P, it then fills the annular groove formed by the spool and the housing, and it flows into the hole (c) drilled
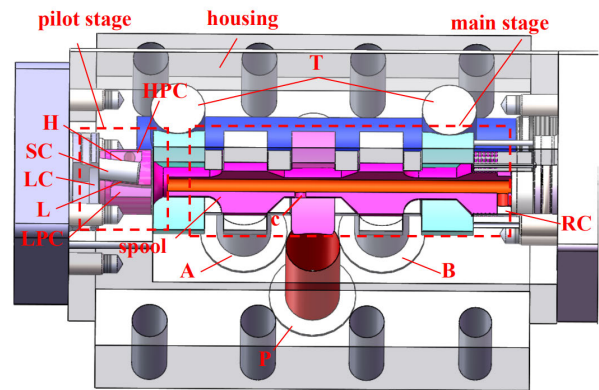

FIGURE 1. A 3D model of the 2D servo valve considered, where A and B are the working ports, P is the inlet port, and T is the return port.

through the centre rod of the spool. After this, the fluid enters the high-pressure cavity (HPC) and the right cavity (RC), respectively, through a long blind hole within the spool. The opening area of orifice H formed by the HPC and the spiral channel (SC) in null state is identical to that of orifice L, formed by the spiral channel and low-pressure cavity (LPC), so the SC pressure is half the value at port P. As the left cavity (LC) is connected directly to the SC, the pressure of the LC is half the RC's. The circular portion of the left end is designed to be twice the size of the annular area in the RC of the spool, so the axial forces on the spool that are produced by the LC and RC pressure are equal at the null position and the spool is stationary.

When the spool is manipulated anticlockwise into an angle by its actuator, the opening area of orifice H is larger than that of orifice L; thereby, the LC pressure rises. The force at the left end of the spool becomes greater than that at the right acting on the annular surface in the RC. In consequence, the spool slides to the right. Then, the annular orifice formed between ports P and B opens, and another orifice, formed between ports A and T, opens at the same time. This state is maintained until the opening areas of orifices H and L in the pilot stage become the same again. If the spool rotates clockwise, the spool's operation is *vice versa*.

B. FLOW FORCES ON THE SPOOL AT THE ANNULAR ORIFICE
The annular orifice between ports P and B opens after the spool slides to the right. The fluid control volume of this path has been selected for calculation of the flow force acting on the spool from a jet discharging into port B. Fig. 2 shows a partial schematic diagram of the main stage and the control volume of the spool cavity, which is filled in grey color. This control volume allows fluid to enter the cut groove connected with port P, then pass into the groove connected with port B after the vena contracta. The formulae for the radial and axial steady flow forces caused by the fluid flows across the orifice can be expressed in terms of the following equations (1) and (2) on the basis of the momentum theory [9]:

$$F_r = 2C_q C_v \pi D x \Delta p \sin\theta \qquad (1)$$
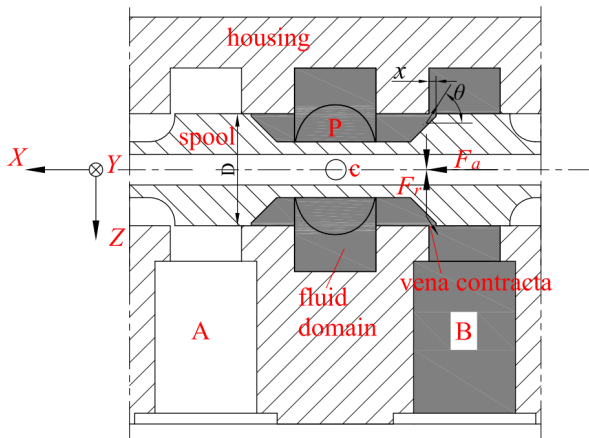$$F_a = 2C_q C_v \pi D x \Delta p \cos\theta \qquad (2)$$

FIGURE 2. A sectional drawing of the main stage.

FIGURE 3. The computational domain and grid.

where F_r is the radial flow force, in newtons (N); F_a is the axial flow force, also in newtons; C_q is the flow coefficient; C_v is the velocity coefficient; D is the shoulder diameter of the spool, in metres (m); x is the opening of the annular orifice, in metres; Δp is the pressure difference, in pascals (Pa); and θ is the jet angle, referring to the acute angle between the velocity at the vena contracta and the X direction.

III. NUMERICAL MODELLING
A. GEOMETRY
The fluid domain of the P–B flow path is chosen for analysis of the radial flow force at the annular orifice of the 2D servo valve. The 3D control volume is shown in Fig. 3. Both the inlet and the outlet passage have a diameter of 20 mm, and the diameter of the shoulder and rod of the spool are, respectively, 24 mm and 11 mm. The depth of the groove in the housing is 7 mm, and the width is 16 mm. For the control surface of the spool shoulder that forms the annular orifice with the groove, a conical shape is maintained, per the design shown in Fig. 2. According to Lugowski [19], this conical control surface for the spool shoulder compensates for the axial steady flow force better than a traditional annular plane does. For the model, the unstructured tetrahedral mesh of the computational domain was created via the grid generator of ANSYS Workbench 19.0.

To investigate the mesh-independence, we generated four unstructured meshes, with 0.38, 0.87, 2.07, and 6.30 million computation cells, labelled as grids 1 to 4 in Fig. 4, and performed simulation for a valve opening x of 0.5 mm. We compared the target value – the outlet flow rate – across the four grids. The discretisation error was estimated by means of the procedure presented by Celik *et al.* [26]. The estimated discretisation error bars are shown in Fig. 4, with the error value presented in brackets. This comparison led us to select Grid 3 for the simulation: it yielded similar values for flow rate to the more computationally demanding Grid 4, in addition to which the numerical uncertainty corresponding to the flow rate solution for the fine grid (Grid 3) was only 0.15%. Thus, the findings from grid-independence analysis
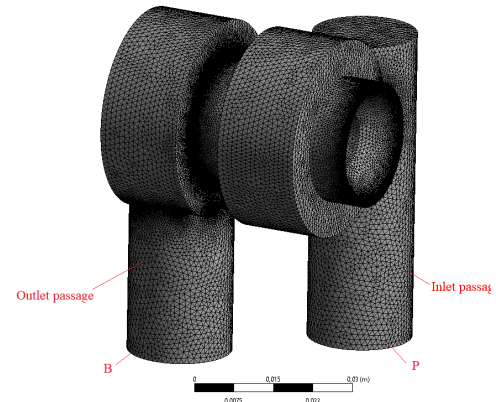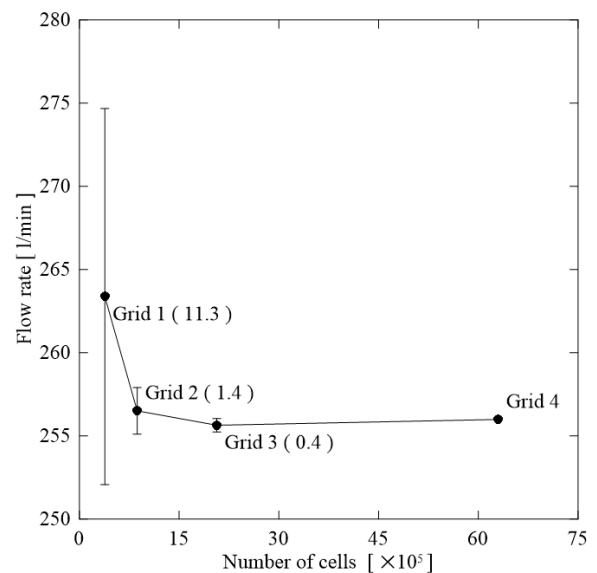

FIGURE 4. The flow rate comparison for grid-independence analysis ($x = 0.5$ mm, the inlet velocity is set to 10 m/s, and outlet pressure is set to 5 MPa).

(see Fig. 4) led us to choose the mesh strategy of Grid 3 for other valve opening conditions.

B. GOVERNING EQUATIONS AND THE SOLUTION STRATEGIES
The steady-state Reynolds-averaged Navier–Stokes (RANS) equations were solved via the commercial CFD application ANSYS Fluent. The $k - \varepsilon$ turbulence model was used to predict turbulence because it accounts for low Reynolds number effects and swirling. The flow was treated as turbulent since the lowest Reynolds number in the domain is 439, which is greater than the critical Reynolds numbers for the spool valve, ranging from 200 to 300 [27]. The enhanced wall treatment (EWT) technique was employed for the work presented here because the y^+ range for the boundary layers of the relevant mesh is 13 to 27, and EWT is insensitive to the non-dimensional distance y^+ and covers intermediated y^+ value in the buffer layer ($5 < y^+ < 30$).

TABLE 1. The boundary-condition and opening values selected for simulation.

Simulation element	Values
Outlet pressure [MPa]	5, 10
Inlet velocity [m/s]	2.5, 5, 7.5, 10, 15
Opening [mm]	0.5, 1, 2, 3, 4, 5

The governing equations were solved with a pressure-based solver. The SIMPLE and PRESTO! schemes were applied, for the pressure–velocity coupling and pressure discretisation, respectively. We utilised the second-order upwind scheme for handling the momentum, turbulent kinetic energy, and turbulent dissipation equations. The velocity inlet was set to be the inlet boundary condition, and the pressure outlet was specified as the outlet boundary condition. For the density and kinetic viscosity of the fluid (ISO VG 46), we used 889 kg/m^3 and 4.5×10^{-5} m^2/s, respectively.

Simulations were conducted for several openings, inlet velocities, and outlet pressure; Table 1 lists the values for the boundary conditions and opening sizes. For the internal flow in the modelling, we regarded the inlet flow as fully developed, so a turbulence intensity and hydraulic diameter specification method was chosen for the calculations. The hydraulic diameter was specified as equal to the diameter of the inlet port, and the value chosen for the turbulence intensity was 6.5 per cent, as the value estimated via the empirical correlation formula, below, varied from 5.2 to 6.5 per cent as the inlet velocity was decreased.

$$I \equiv u'/u_{avg} = 0.16(R_{eD_H})^{-1/8} \tag{3}$$

Here, I denotes the turbulence intensity, which is defined as the ratio of the root mean square of the velocity fluctuations, u', to the mean flow velocity, u_{avg}, and R_{eD_H} is the Reynolds number.

IV. RESULTS AND DISCUSSION

The radial flow force caused by the fluid flowing through the annular orifice is distributed over the round edge of the spool. Therefore, we selected four critical sections for purposes of collecting the relevant simulation data for pressure and jet angle θ at each position angle α. These are referred to as the 0°–180°, 45°–225°, 90°–270°, and 135°–315° sections. They are depicted in Fig. 5.

As the fluid converges into the orifice, pressure drops rapidly as the flow velocity rises. The changes in the velocity's magnitude and direction generate flow force acting on the spool, with prior research [19] pointing to an effective range of 1 mm downstream from the orifice. Therefore, in our work, the pressure value was retrieved for planes P_{up} and P_{down}, maintaining a distance of 0.8 mm upstream and downstream of the control edge of the orifice, respectively, as shown in Fig. 6.

A. THE EFFECT OF OUTLET PRESSURE

Fig. 7 presents the annular distributions of pressures over planes P_{up} and P_{down} and jet angle θ for the two outlet pressures 10 MPa and 5 MPa. The orifice opening is 0.5 mm, and the inlet velocity is 5 m/s.
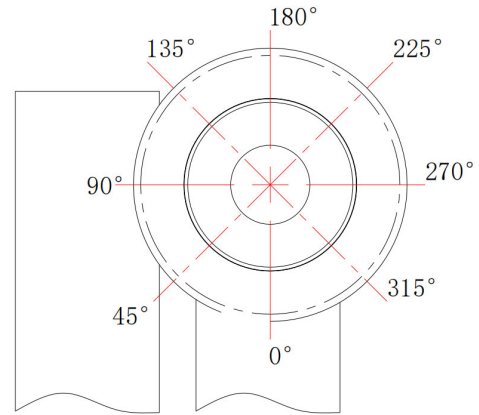

FIGURE 5. The position of the four critical sections selected.
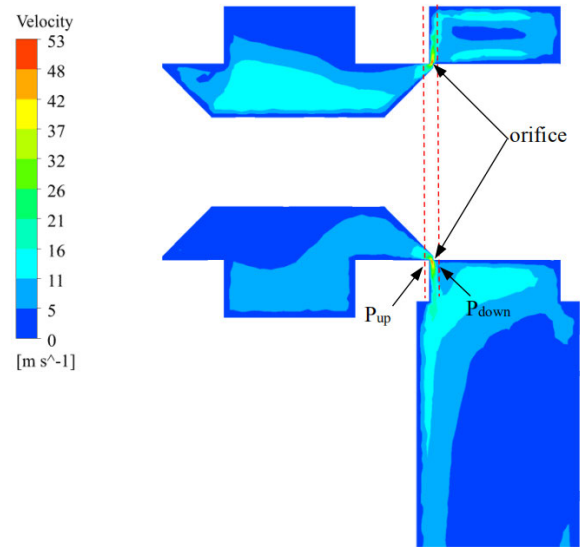

FIGURE 6. The velocity contour of the 0°–180° section.

In Fig. 7, the smallest values for the jet angle are oriented toward the outlet passage direction, where α is 0°. The jet angle remains constant for the rest of the annular orifice. We calculated the radial flow forces at the various positions in accordance with formula (1), for which the flow coefficient (C_q) and velocity coefficient (C_v) were set to 0.61 and 0.98 [25], respectively. The two curves in Fig. 8 represent the circumferential distribution of the radial flow force under different outlet pressure conditions. These two curves for around the orifice are almost entirely congruent, it is evident from this result that the radial flow force acting on the spool is not affected by the outlet pressure.

B. THE EFFECT OF INLET VELOCITY

The effect of the inlet velocity on the radial force was studied at five values: 2.5 m/s, 5 m/s, 7.5 m/s, 10 m/s, and 15 m/s, with the orifice opening kept steady at 0.5 mm and the outlet pressure at 5 MPa. Fig. 9 shows five curves, one for each of these velocities, for the pressure difference around the annular orifice between P_{up} and P_{down}. There is a noticeable
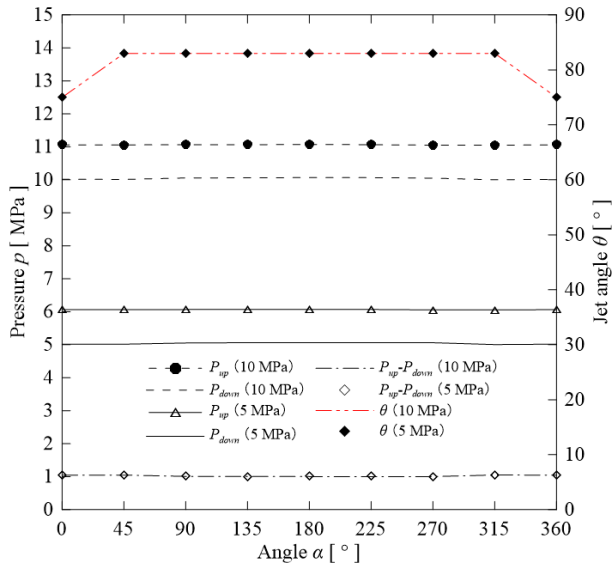
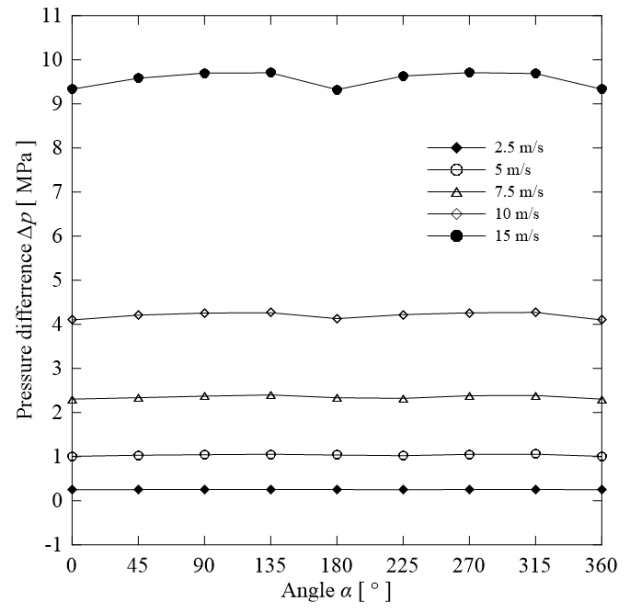**FIGURE 7.** Pressure and jet angle distributions at various outlet pressures.

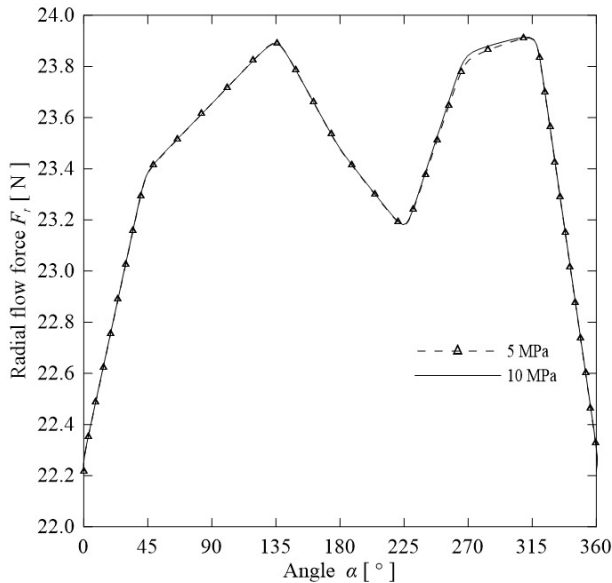**FIGURE 8.** Circumferential distribution of radial flow force under two sets of outlet pressure conditions.

FIGURE 9. Pressure difference at different inlet velocities.

FIGURE 10. Radial flow force distributions for various inlet flow velocities.

increase in the pressure difference as the inlet flow velocity rises, and that value is proportional to the square of inlet flow velocity. By means of the following equations (4) and (5), this could be explained in terms of mass and energy conservation [28], [29]:

$$Q_{in} = A_{in}v_{in} = A_q A_0 \sqrt{\frac{2}{\rho}\Delta p} \tag{4}$$

where Q_{in} is the inlet flow rate, given in m^3/s; A_{in} is the area of inlet port P, in m^2; and A_o is the area of the orifice, in m^2.

Accordingly, Δp can be expressed as

$$\Delta p = \frac{\rho}{2}\left(\frac{A_{in}}{C_d A_0}\right)^2 v_{in}^2 = \rho C v_{in}^2 \tag{5}$$
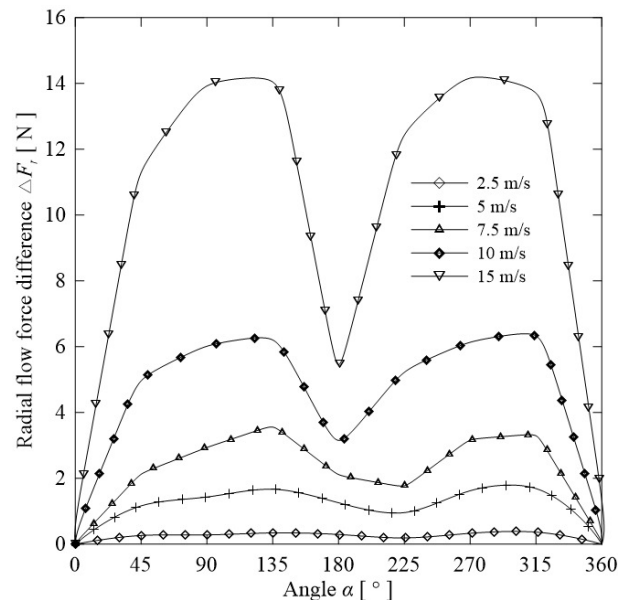
Here, C, or $\frac{1}{2}\left(\frac{A_{in}}{C_d A_0}\right)^2$, is constant when flow coefficient C_d and the areas of inlet port A_{in} and orifice A_o remain unchanged.

The radial flow forces under the five distinct inlet velocities were calculated on the basis of formula (1) from the data presented in Fig. 9, and Fig. 10 presents the five corresponding curves for radial flow force difference ΔF_r, which were obtained by using absolute radial flow forces to subtract out the minimum value for each condition. Table 2 presents the amplitudes of radial flow force F_{ra} for the various inlet velocities, and the trend of increase in F_{ra} with inlet velocity is shown in Fig. 11. For our calculations, we used the r_i ratio,

TABLE 2. The amplitudes of radial flow force F_{ra} with various values for inlet flow velocity v_{in}.

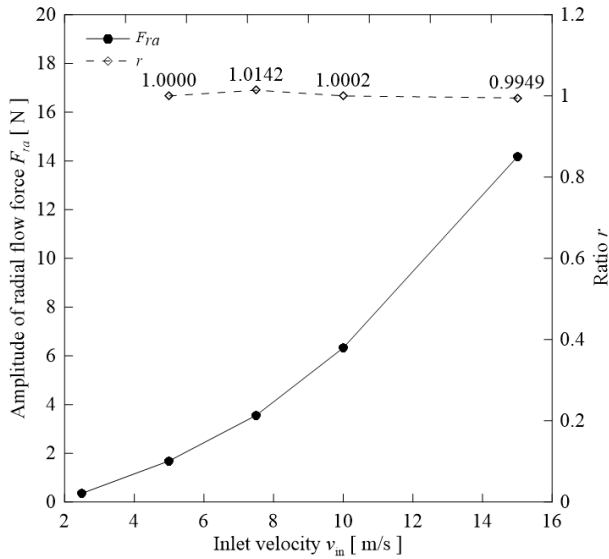| Serial number n	v_{in} [m/s]	F_{ra} [N]
1	2.5	0.39
2	5	1.56
3	7.5	3.56
4	10	6.33
5	15	14.17

FIGURE 11. The relationship between inlet velocity and the amplitude of radial flow force.

defined as the ratio of radial flow force amplitude F_{ra} to the square of the inlet flow velocity. This is calculated thus:

$$r_i = r_{n+1} = \left(\frac{F_{ra}(n+1)}{F_{ra}(n)}\right) \bigg/ \left(\frac{v_{in}(n+1)}{v_{in}(n)}\right)^2 \qquad (6)$$

where n refers to the serial number listed in Table 2. The four values of r_i presented in Fig. 11 are calculated for $n = 1$ to $n = 4$. That the r_i curve for the value of 1 is close to a horizontal straight line illustrates the fact that the amplitude of radial flow force is proportional to the square of inlet flow velocity, which can be verified by substituting formula (5) into formula (1).

C. THE EFFECT OF THE ORIFICE OPENING
Fig. 12 shows radial flow forces for four orifice opening values – namely, 1 mm, 2 mm, 3 mm, and 4 mm – when the outlet pressure is 5 MPa and inlet velocity is 10 m/s. The curves demonstrate that the radial flow force decreases as the orifice opening grows. The radial flow force exhibits a reciprocal relationship with the orifice opening, as attested by (7), which is derived from the above-mentioned substitution.

$$F_r = \frac{\rho C_v A_{in}^2 v_{in}^2 \sin\theta}{C_d \pi D x} \qquad (7)$$

The amplitude values of the four curves shown in Fig. 12 as the opening expands from 1 mm to 4 mm are 6.08 N, 7.03 N, 9.17 N, and 9.85 N.
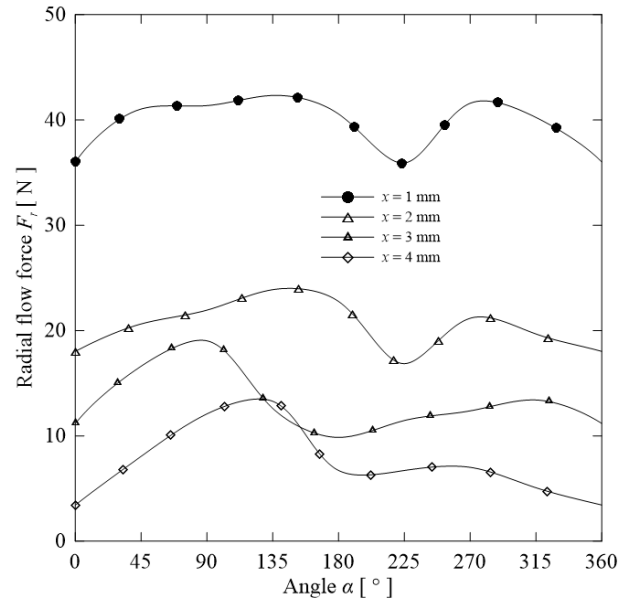

FIGURE 12. Radial flow force distribution for various openings.

D. RADIAL FORCE
To study the radial force acting on the spool in response to the asymmetrical radial flow force at the annular orifice, one can calculate the net radial force by projecting the radial flow force in the Y and Z direction and summing in the same direction to find the square roots. The components of the net radial force in the Y and Z direction can be calculated as, respectively,

$$F_{rY} = -\sum F_r(\alpha)\sin\alpha \qquad (8)$$

$$F_{rZ} = -\sum F_r(\alpha)\cos\alpha \qquad (9)$$

where F_{rY} is the Y component of the net radial force and F_{rZ} is the Z component. Net radial force F_r' acting on the spool at the orifice is the square root of the F_{rY} and F_{rZ} values, per formula (10), and the angle of the radial force to the positive direction of the z-axis α can be calculated via (11):

$$F_r' = \sqrt{F_{rY}^2 + F_{rZ}^2} \qquad (10)$$

and

$$\alpha = \begin{cases} \pi + \text{atan}\dfrac{F_{rY}}{F_{rZ}} & F_{rY} > 0, \ F_{rZ} > 0 \\[2mm] 2\pi + \text{atan}\dfrac{F_{rY}}{F_{rZ}} & F_{rY} > 0, \ F_{rZ} < 0 \\[2mm] \pi + \text{atan}\dfrac{F_{rY}}{F_{rZ}} & F_{rY} < 0, \ F_{rZ} > 0 \\[2mm] \text{atan}\dfrac{F_{rY}}{F_{rZ}} & F_{rY} < 0, \ F_{rZ} < 0 \end{cases} \qquad (11)$$

As the radial flow force distributions are not circumferentially symmetrical at the annular orifice, the distribution trend is plotted to show how the radial flow force varies around the orifice. Fig. 13 presents the distribution of radial flow force around the orifice for one sample condition, to illustrate its asymmetry. For this condition, the net radial force and angular
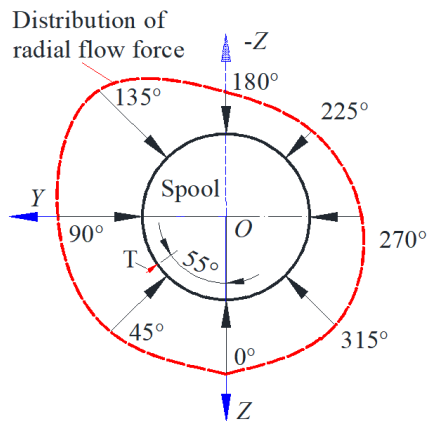
FIGURE 13. The circumferential distribution of radial flow force at the annular orifice and the corresponding net radial force when *x* is 4 mm and v_{in} is 10 m/s.

TABLE 3. Net radial force F_r' and its angular position α.

Opening x [mm]	Inlet velocity v_{in} [m/s]	F_r' [N]	α [°]
0.5	2.5	0.25	359
0.5	5	1.06	0
0.5	7	2.27	353
0.5	10	3.64	4
0.5	15	7.35	4
1	10	5.01	11
2	10	8.91	26
3	10	11.18	31
4	10	14.38	55

position are, respectively, 14.38 N and 55°, denoted by 'T'. As the changing of outlet pressure has no contribution to the distribution of radial flow force, only different openings and inlet velocities are chosen as variable factors. The net radial force values and angular positions of nine different conditions are filled in Table 3.

The values in Table 3 indicate that the radial force increases as the inlet flow velocity grows, when the opening and outlet pressure are constant. This is because of the asymmetric distribution of radial flow force. Also, the amplitude of that force grows with the inlet velocity, as shown in Figs. 10 and 11. The net radial force is greater when the opening is equal to or larger than 1 mm, relative to that with a 0.5 mm opening at the same inlet velocity and outlet pressure. The magnitude of the net radial force changes with the opening size, which is also affected by the amplitude and symmetry of the radial flow force. The net radial force manifests itself near 0° and is oriented in the negative direction on the *z*-axis when the opening size is 0.5 mm. When the opening is at least 1 mm, the net radial force appears in the lower-left quadrant with reference to Fig. 13. Therefore, one can conclude that the direction of the total radial force changes with the opening of the orifice, and the direction moves from the negative *Z* direction to negative *Y*.

The results presented above illustrate that the radial force induced when fluid flows through the orifice must not be neglected for large openings or cases of high inlet velocity, because the net radial force could lead to spool eccentricity

or tilting of the bore centre line, which generates extra friction resistance in the process of sliding.

V. CONCLUSION

Valuable results emerged from this research into 1) the radial flow force's distribution and its effects around the annular orifice of the main stage of a 2D servo valve and 2) the net radial force acting on the spool in consequence of the fluid flows. Firstly, the results indicate that the radial flow force arises from the asymmetric fluid cavity, while outlet pressure had no effect on that force's distribution. Our work demonstrated that the radial flow force distribution is affected by the inlet flow velocity and the opening of the orifice, with the amplitude of the radial flow force increasing linearly with the square of inlet velocity and showing an inverse relationship with the opening size. The net radial force acting on the spool was verified as not representing mutual cancellation of the forces, and it grew with the inlet flow velocity and the orifice size. These results can inform not only analysis of the radial force operating at the main stage of a 2D servo valve but also work with traditional slide valves with a conical side surface.

Further research should focus on experiments to validate the numerical results presented in this paper. We would recommend modifying the model of the valve's dynamics so as to account for the effect of the radial flow force. With a model modified thus, new structures for slide valves could be designed, enabling better compensation for both axial and radial flow forces. Thereby, better valve performance should be produced.

REFERENCES

[1] J. Ruan, R. Burton, and P. Ukrainetz, "An investigation into the characteristics of a two dimensional '2D' flow control valve," *J. Dyn. Syst., Meas., Control*, vol. 124, no. 1, pp. 214–220, Mar. 2002.

[2] J. Ruan, S. Li, X. Pei, R. Burton, P. R. Ukrainetz, and D. Bitner, "2D digital simplified flow valve," *Chin. J. Mech. Eng-EN*, vol. 17, no. 3, pp. 311–314, 2004.

[3] R. Burton, J. Ruan, and P. Ukrainetz, "Analysis of electromagnetic nonlinearities in stage control of a stepper motor and spool valve," *J. Dyn. Syst., Meas., Control*, vol. 125, no. 3, pp. 405–412, Sep. 2003.

[4] L. Sheng, R. Jian, and M. Bin, "Research for the characteristics of electromechanical converter for 2D digital servo valve," in *Proc. IEEE 10th Int. Conf. Ind. Informat.*, Jul. 2012, pp. 719–724.

[5] H. Jiang, J. Ruan, S. Li, X. Zuo, and Y. Chen, "Design and experiment of 2D electrohydraulic high-speed on–off valve," (in Chinese), *Trans. Chin. Soc. Agricult. Machinery*, vol. 46, no. 2, pp. 328–334, 2015.

[6] G. Liu, J. Ruan, S. Li, and B. Meng, "Design and experimental study of two-dimensional(2D) electro-hydraulic proportional directional valve," in *Proc. Int. Conf. Fluid Power Mechatronics (FPM)*, Aug. 2015, pp. 276–282.

[7] S. Li, J. Ruan, and B. Meng, "Two-dimensional electro-hydraulic proportional directional valve," (in Chinese), *J. Mech. Eng.*, vol. 52, pp. 202–212, 2016.

[8] Q. Yuan and P. Y. Li, "Using steady flow force for unstable valve design: Modeling and experiments," *J. Dyn. Syst., Meas., Control*, vol. 127, no. 3, pp. 451–462, Sep. 2005.

[9] N. Herakovič, "Flow-force analysis in a hydraulic sliding-spool valve," *Strojarstvo*, vol. 51, no. 6, pp. 555–564, 2009.

[10] J. Rajda and E. Lisowski, "Flow forces acting on the spool of directional control valve," *Czasopismo Techniczne. Mechanika*, vol. 5, no. 1, pp. 349–356, 2013.

[11] E. Frosina, A. Senatore, D. Buono, M. Pavanetto, and M. Olivetti, "3D CFD transient analysis of the forces acting on the spool of a directional valve," *Energy Procedia*, vol. 81, pp. 1090–1101, Dec. 2015.

[12] E. Frosina, G. Marinaro, A. Senatore, and M. Pavanetto, "Numerical and experimental investigation for the design of a directional spool valve," *Energy Procedia*, vol. 148, pp. 274–280, Aug. 2018.

[13] R. Amirante, L. Andrea Catalano, and P. Tamburrano, "The importance of a full 3D fluid dynamic analysis to evaluate the flow forces in a hydraulic directional proportional valve," *Eng. Comput.*, vol. 31, no. 5, pp. 898–922, Jul. 2014.

[14] R. Amirante, E. Distaso, and P. Tamburrano, "Sliding spool design for reducing the actuation forces in direct operated proportional directional valves: Experimental validation," *Energy Convers. Manage.*, vol. 119, pp. 399–410, Jul. 2016.

[15] M. Han, Y. Liu, D. Wu, H. Tan, and C. Li, "Numerical analysis and optimisation of the flow forces in a water hydraulic proportional cartridge valve for injection system," *IEEE Access*, vol. 6, pp. 10392–10401, 2018.

[16] H. Xie, L. Tan, J. Liu, H. Chen, and H. Yang, "Numerical and experimental investigation on opening direction steady axial flow force compensation of converged flow cartridge proportional valve," *Flow Meas. Instrum.*, vol. 62, pp. 123–134, Aug. 2018.

[17] L. Tan, H. Xie, H. Chen, and H. Yang, "Structure optimization of conical spool and flow force compensation in a diverged flow cartridge proportional valve," *Flow Meas. Instrum.*, vol. 66, pp. 170–181, Apr. 2019.

[18] D. Qu, Y. Zhou, Y. Liu, W. Luo, and F. Zhang, "Steady flow force compensation and test research on electrohydraulic proportional relief valve," *IEEE Access*, vol. 7, pp. 48087–48097, 2019.

[19] J. Lugowski, "Flow force in a hydraulic spool valve," in *Proc. ASME-JSME-KSME Joint Fluids Eng. Conf.*, San Francisco, CA, USA, Aug. 2019, pp. 1–9.

[20] L. Lu, F. Xia, Y. Yin, J. Yuan, and S. Guo, "Spool stuck mechanism of ball-type rotary direct drive pressure servo valve," (in Chinese). *J. ZheJiang Univ., Eng. Sci.*, vol. 53, no. 7, pp. 1265–1273, 2019.

[21] Y. Zhang, S. Wang, J. Shi, and X. Wang, "Evaluation of thermal effects on temperature-sensitive operating force of flow servo valve for fuel metering unit," *Chin. J. Aeronaut.*, vol. 33, no. 6, pp. 1812–1823, Jun. 2020.

[22] X. Zhang, X. Pei, P. Lv, S. Yang, and J. Ruan, "Research and analysis of forces on a 2D digital valve spool," (in Chinese), *Fluid Power Trans. Cont.*, vol. 6, pp. 16–18, Nov. 2011.

[23] Q. Lu, J. Ruan, and S. Li, "Study on steady-state flow force of pilot helical orifice of 2D servo valve," (in Chinese), *Fluid Machinery*, vol. 47, no. 1, pp. 25–30, 2019.

[24] *Hydraulic Fluid Power—Four- and Five-Port Servovalves—Mounting Surfaces*, Standard ISO 10372:1992, International Organization for Standardization, Geneva, Switzerland, R2017.

[25] N. D. Manring and R. C. Fales, *Hydraulic Control Systems*. Hoboken, NJ, USA: Wiley, 2019.

[26] I. B. Celik, U. Ghia, P. J. Roache, and C. J. Freitas, "Procedure for estimation and reporting of uncertainty due to discretization in CFD applications," *J. Fluids Eng.-Trans. ASME*, vol. 130, no. 7, 2008.

[27] H. Sigloch, *Technische fluidmechanik*, vol. 6. Berlin, Germany: Springer, 2017.

[28] M. K. Oshtorjani, A. Mikkola, and P. Jalali, "Numerical treatment of singularity in hydraulic circuits using singular perturbation theory," *IEEE/ASME Trans. Mechatronics*, vol. 24, no. 1, pp. 144–153, Feb. 2019.

[29] J. Rahikainen, M. Kiani, J. Sopanen, P. Jalali, and A. Mikkola, "Computationally efficient approach for simulation of multibody and hydraulic dynamics," *Mechanism Mach. Theory*, vol. 130, pp. 435–446, Dec. 2018.

QIANQIAN LU was born in Anhui, China, in 1985. She received the bachelor's degree in mechanical design and automation from Northeastern University, Shenyang, China, in 2007, the M.Sc. degree in mechatronics engineering from China's Zhejiang University, Hangzhou, in 2010, and the Ph.D. degree from the School of Mechanical Engineering, Zhejiang University of Technology, Hangzhou, in 2019.

Since 2010, she has worked as a Lecturer at the Hangzhou's Zhejiang University City College. She is currently a Visiting Scholar with the Finland's Lappeenranta–Lahti University of Technology (LUT). Her current research interests include fluid mechanics, computational fluid dynamics, hydraulic components, and hydraulic transmission and control.

JONNA TIAINEN was born in Mikkeli, Finland, in 1990. She received the B.Sc., M.Sc., and D.Sc. degrees in energy systems from the Lappeenranta University of Technology, in 2012, 2014, and 2018, respectively.

Since 2018, she has been active as a Postdoctoral Researcher with the Lappeenranta–Lahti University of Technology, where her research concentrates on turbomachinery. Among her key research interests are energy-storage technologies and cavitation of cryogenic fluids.

MEHRAN KIANI-OSHTORJANI was born in Isfahan, Iran, in 1991. He received the B.Sc. degree from Yazd University, in 2013, and the M.Sc. degree from the Sharif University of Technology, in 2015. He is currently pursuing the Ph.D. degree with LUT, Finland.

His areas of scientific research include fluid power systems, real-time simulation, the dynamic and thermal behavior of granular materials, and multi-phase flows. He is an expert in carrying out real-time simulations, both as an Algorithm Designer and as a professional Scientific Programmer.

JIAN RUAN was born in Fujian, China, in 1963. He received the B.Sc., M.Sc., and Ph.D. degrees from the Harbin Institute of Technology, China, in 1983, 1986, and 1989, respectively.

He worked as a Postdoctoral Fellow at the Institute of Fluid Power Transmission and Control (FTPC), Zhejiang University, from 1989 to 1992. He currently holds a professorship in electrical and mechanical engineering with the Zhejiang University of Technology, where fluid power control, dynamic systems, and the design and development of two-dimensional hydraulic components are among his many research interests.

• • •